Clays and Clay Minerals, Vol. 56, No. 1, 100–111, 2008.

DIAGENETIC REORIENTATION OF PHYLLOSILICATE MINERALS IN PALEOGENE MUDSTONES OF THE PODHALE BASIN, SOUTHERN POLAND

RUARRI J. DAY-STIRRAT[1,4], ANDREW C. APLIN[1,*], JAN ŚRODOŃ[2], AND BEN A. VAN DER PLUIJM[3]

[1] School of Civil Engineering and Geosciences, Drummond Building, Newcastle University, Newcastle upon Tyne NE1 7RU, UK
[2] Institute of Geological Sciences, Polish Academy of Sciences, Senacka 1, 31-002 Kraków, Poland
[3] Department of Geological Sciences, University of Michigan, C.C. Little Building, 425 E. University Ave., Ann Arbor, MI 48109-1063, USA

Abstract—We used high-resolution X-ray texture goniometry to quantify changes in the mm-scale orientation of phyllosilicate minerals in a suite of Paleogene mudstones from the Podhale Basin in southern Poland. The sample set covers an estimated range of burial depths between 2.4 and 7.0 km, corresponding to a temperature range of 60–160ºC. Although mechanical compaction has reduced porosities to ~10% in the shallowest samples, the phyllosilicate fabric is only modestly aligned. Coarser-grained (>10 μm) detrital chlorite and mica appear to be more strongly aligned with (001) parallel to bedding, suggesting their deposition as single grains rather than as isotropic flocs or aggregates. From 2.4 to 4.6 km, R0 illite-smectite with 40–50% illite layers changes to R1 illite-smectite with 70–80% illite layers. At the same time kaolinite is lost and diagenetic chlorite is formed. The mineralogical changes are accompanied by a strong increase in the alignment of illite-smectite, chlorite, and detrital illite, parallel to bedding and normal to the presumed principal effective stress. We propose that the development of a more aligned I-S fabric results from the dissolution of smectite and the growth of illite with (001) normal to the maximum effective stress. Water released by illitization may act as a lubricant for the rotation of all platy minerals into nanoporosity transiently formed by the illitization reaction. At greater depths and temperatures, further illitization is inhibited through the exhaustion of K-feldspar. After the cessation of illitization, a further 2.4 km of burial only results in a small increase in phyllosilicate alignment. At such small values for porosity and pore size, increasing stress does not substantially reorient phyllosilicates in the absence of mineralogical change.

Key Words—Diagenesis, Fabric, Mudstone, Phyllosilicate, Shale, Textural Goniometry.

INTRODUCTION

In the marine environment, particles are sedimented by two main processes: grains >~10 μm in diameter are deposited largely by settling of single grains, while grains of <10 μm are deposited mainly as flocs or as biologically produced aggregates (*e.g.* Kranck and Milligan, 1985; O'Brien and Slatt, 1990; Kranck *et al.*, 1996). These depositional processes may be expected to produce an essentially isotropic fabric for fine-grained (<10 μm) phyllosilicates (Bennett *et al.*, 1991) but a more anisotropic fabric for coarse, silt-grade phyllosilicates such as mica and chlorite. The initial, depositional fabric is then profoundly transformed by diagenesis and low-grade metamorphism into the highly aligned fabric observed in low-grade metamorphic pelites (*e.g.* Jacob *et al.*, 2000).

Although the reorientation of phyllosilicate minerals is a fundamental diagenetic process, the mechanisms of reorientation are poorly understood. In particular, the relative roles of mechanical loading and grain rotation (*e.g.* Hedberg, 1936; Bowles *et al.*, 1969; Vasseur *et al.*, 1995) *vs.* clay mineral recrystallization (Ho *et al.*, 1999; 2001) have not been evaluated properly. With notable exceptions (Oertel and Curtis, 1972; Curtis *et al.*, 1980; Ho *et al.*, 1999; Worden *et al.*, 2005; Aplin *et al.*, 2006), very few studies have attempted to quantify phyllosilicate fabric and to monitor its evolution as a function of both the mechanical and chemical processes operating through the diagenetic realm.

In this study we report how high-resolution X-ray texture goniometry (HRXTG) (van der Pluijm *et al.*, 1994) has been used to quantify changes in the alignment of phyllosilicates during the deep burial diagenesis of a series of Lower Tertiary mudstones from the Podhale Basin in Poland. The relative homogeneity of the samples (Środoń *et al.*, 2006) minimizes the influence of quartz/clay ratio as a control on fabric alignment (Curtis *et al.*, 1980) and allows us to focus on the relative importance of mechanical stress and mineral recrystallization, specifically the conversion of smectite to illite, on fabric development.

* E-mail address of corresponding author:
a.c.aplin@ncl.ac.uk
[4] Present address: Bureau of Economic Geology, John A. and Katherine G. Jackson School of Geosciences, The University of Texas at Austin, University Station, Box X, Austin, TX 78713-1534, USA
DOI: 10.1346/CCMN.2008.0560109

SETTING AND SAMPLES

The Paleogene Podhale Basin of southern Poland is situated between the Pieniny Klippen Belt to the north and the Tatra Mountains to the south (Figure 1), and is part of the much larger, Central Carpathian Paleogene Basin. The basin is thought to have formed in a fore-arc setting at the north-east border of the North-Pannonian unit (Tari *et al.*, 1993). Currently, the basin has a sequence of up to 3000 m of sandstones, mudstones, and siltstones, termed the Podhale Flysch (Olszewska and Wieczorek 1998), covering a Mesozoic basement that is exhumed in the Tatra Mountains.

The sample set consists of 19 fragments of cores taken from two boreholes in the Podhale Basin: Chochołów PIG-1 in the west and Bukowina Tatrzańska PIG-1 in the east. Chochołów PIG-1 comprises the Chochołów (two samples), Zakopane (six samples), and Szaflary beds (three samples), whereas Bukowina Tatrzańska consists of only the Chochołów (four samples) and Zakopane beds (four samples). Olszewska and Wieczorek (1998) described the Szaflary beds as Late Eocene clastic deposits rare in foraminifera, deposited along a tectonically controlled submarine ramp. The Zakopane beds comprise mainly dark shales, a generally upwards-coarsening sequence related to submarine fan sedimentation, with minor intercalations of thin-bedded sandstones and local intercalations of ferruginous dolomites. The Chochołów beds are siliciclastic deposits deposited in a similar setting to the Zakopane beds. Samples were chosen based on similarity in terms of color, apparent grain size, and bedding characteristics at the hand specimen scale, to represent entire lengths of the two profiles. They are exactly the same samples as used in a parallel study of mineral diagenesis in the Podhale Basin (Środoń *et al.*, 2006).

Środoń *et al.* (2006) argued, on the basis of grain-density trends, that the Chochołów PIG-1 and Bukowina Tatrzańska PIG-1 wells can be regarded as a continuous burial profile, with ~500 m overlap. By linking the wells in this way, %S trends in mixed-layer I-S, as well as trends in quartz, albite, chlorite, kaolinite, and K-feldspar are continuous (see figure 8 in Środoń *et al.*, 2006). Both

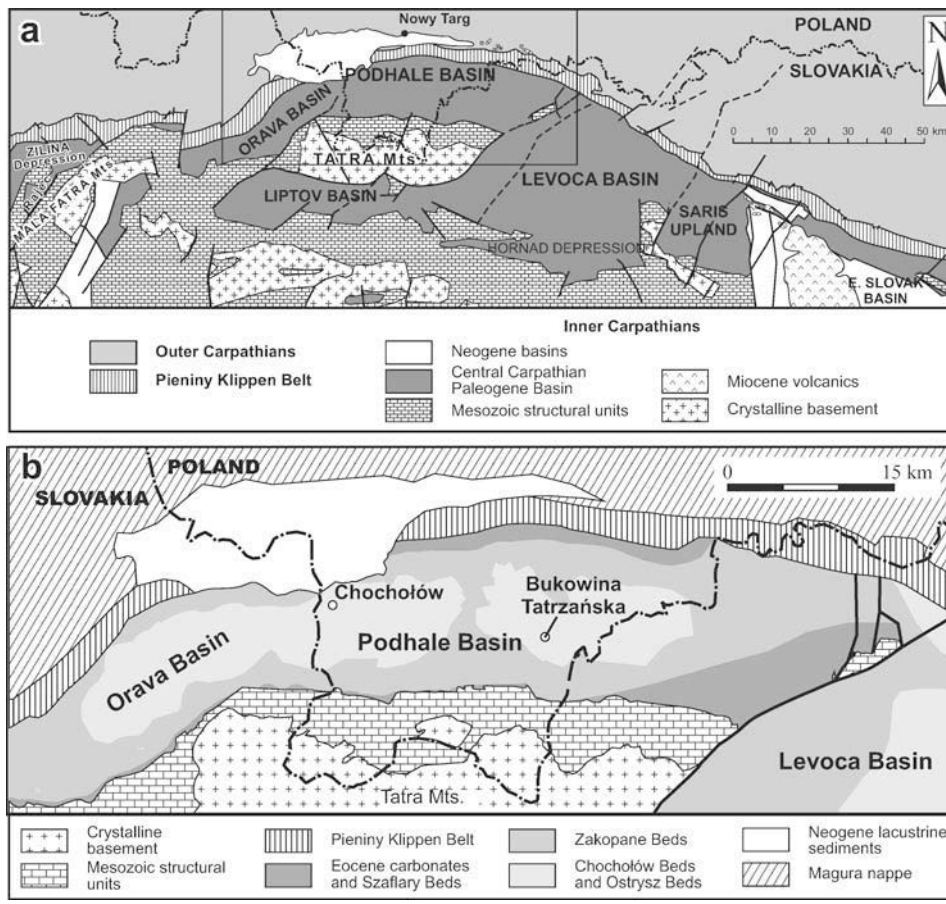

Figure 1. (a) The Podhale Basin with its surrounding sub-basins and major structural faults. (b) The Podhale Basin lithologies and the locations of the Chochołów and Bukowina Tatrzańska wells (adapted from Środoń *et al.*, 2006).

https://doi.org/10.1346/CCMN.2008.0560109 Published online by Cambridge University Press

the present-day and calculated paleo-geothermal gradients are similar in both locations, ~20−25ºC km^{-1}. Thermal maturity data from Poprawa and Marynowski (2005) are consistent with the proposed overlap between the two wells (Środoń *et al.*, 2006). Based on this evidence, the two wells have also been combined into one diagenetic profile in this study. The maximum burial depth of the top of Bukowina Tatrzańska profile was evaluated from %S data as between 4.2 and 5.2 km, *i.e.* an average of 4.7 km (see figure 9 and table 6 of Środoń *et al.*, 2006). This is very close to the value of 4.6 km estimated from apatite fission-track data from the same well (Anczkiewicz, 2006). Based on this number, and assuming a 500 m overlap between the profiles, we estimate the maximum burial at the top of Chochołów as 2.2 km, the value we adopt in this work.

According to K-Ar dates for clay mineral separates from bentonites (Środoń *et al.*, 2006), the maximum burial of the Podhale Basin was achieved ~17 Ma ago, indicative of rapid Eocene to Early Miocene subsidence, especially in the eastern part of the Podhale Basin around Bukowina Tatrzańska. Average sedimentation rates range from 300 m my^{-1} in the west of the basin to 440 m my^{-1} in the east.

Key mineralogical and geochemical data are given in Table 1 and show that most of the samples are similar in bulk composition. Total clay ranges from 46 to 66%, mainly between 50 and 60%; quartz ranges from 16 to 29%, mainly between 20 and 26%; clay/quartz ratios range from 1.9 to 4.3, mainly between 2 and 3.

ANALYTICAL METHODS

X-ray diffraction

The mineralogical composition of these samples was described in detail by Środoń *et al.* (2006), along with the detailed analytical methods. Briefly, quantitative mineralogy was determined using the method described by Środoń *et al.* (2001) and the percentage of smectite in mixed-layer illite-smectite estimated on glycolated and oriented <0.2 μm separates using peak-position methods. The key results are presented in Table 1, and Figure 2 shows X-ray diffraction (XRD) patterns which are representative of the whole range of observed expandability.

BSEM

Two thin sections were made perpendicular to bedding, one for scanning electron microscopy (SEM) observations and another for HRXTG. The section for the SEM observations was prepared with a surface oriented parallel to that of the section for HRXTG, allowing direct comparison. We used an Hitachi S2400 Scanning Electron Microscope equipped with an Oxford Instruments Isis 200 Ultra Thin Window X-ray detector. The machine was operated at 20 kV and 2 nA, with a spot size of 2 μm and a working distance of ~15 mm.

High-resolution X-ray texture goniometry

A quantitative assessment of the alignment of phyllosilicates was made on an Enraf-Nonius CAD4 automated

Table 1. Selected mineralogical data (from Środoń *et al.*, 2006).

Sample	Actual burial depth (m)	Estimated max. burial depth (m)	Quartz (%)	K-feldspar (%)	Kaolinite (%)	2:1 clays (I+M+Fe-S) (%)	Chlorite (%)	Total clay (%)	K_2O (%)	Illite in I-S (%)
Chi-04	193	2393	19.0	2.2	3.2	45.8	0.7	49.7	3.62	48
Chi-06	280	2480	24.3	2.3	1.5	46.8	4.0	52.3	3.56	50
Chi-12	514	2714	18.5	2.2	3.2	50.2	2.6	56.0	3.21	37
Chi-20	821	3021	22.9	1.5	3.6	49.2	2.1	54.9	2.95	53
Chi-23	1031	3231	21.7	1.3	2.9	43.9	2.6	49.4	2.9	55
Chi-28	1283	3483	20.4	0.5	2.6	49.1	3.6	55.3	3.0	56
Chi-38	1671	3871	16.3	1.5	1.0	60.8	7.4	69.2	4.7	76
Chi-44	2012	4212	26.0	1.0	1.0	53.9	5.2	60.1	3.4	68
Chi-56	2410	4610	20.5	0.5	0.8	60.1	4.8	65.7	4.24	73
Chi-60	2611	4811	27.5	0.4	–	41.1	4.7	45.8	2.9	76
Chi-66	2968	5168	22.4	0.5	–	41.8	4.2	46.0	2.9	69
BkT-01	102	4908	26.6	0.8	0.8	53.6	5.6	60.0	3.5	75
BkT-06	294	5100	25.2	0.5	0.5	54.3	5.6	60.4	3.55	76
BkT-12	610	5416	27.0	1.0	–	52.0	6.1	58.1	3.1	74
BkT-17	903	5709	24.1	0.5	–	48.1	3.1	51.2	3.3	75
BkT-23	1261	6067	23.3	1.0	–	50.7	4.2	54.9	3.3	80
BkT-28	1595	6401	27.0	–	–	46.8	4.4	51.2	3.1	70
BkT-35	1904	6710	29.4	0.5	–	50.1	3.6	53.7	3.4	82
BkT-41	2201	7007	26.4	–	–	51.5	4.0	55.5	3.3	76

–: below detection limit

The samples are arranged according to their actual depth and estimated maximum burial depths (see text).

https://doi.org/10.1346/CCMN.2008.0560109 Published online by Cambridge University Press

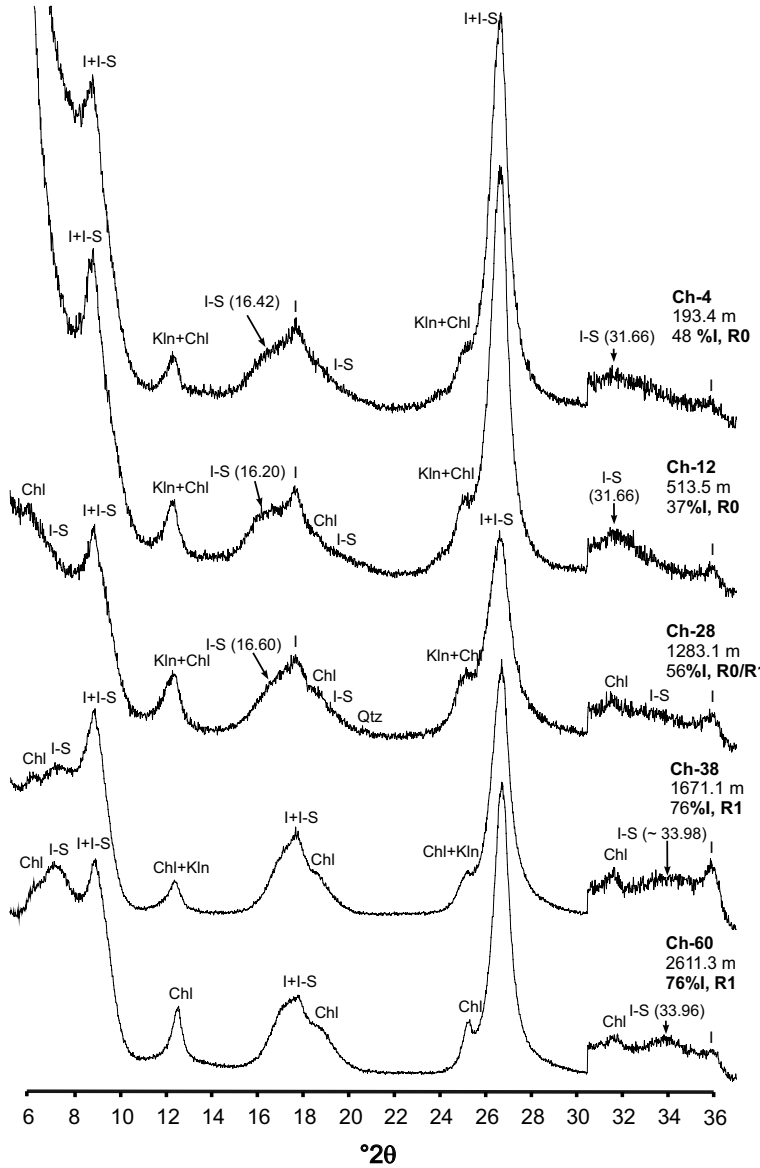

Figure 2. XRD patterns of glycolated oriented preparations of <0.2 μm fractions of selected samples, illustrating the complete range of expandability (modified from Kotarba, 2003). I – discrete illite, I-S – illite-smectite, Kln – kaolinite, Chl – chlorite, Qtz – quartz, R0 – random interstratification, R1 – ordered interstratification. I-S peak positions used by %I quantification techniques, are also given.

single-crystal diffractometer using the HRXTG method described by van der Pluijm *et al.* (1994). The HRXTG analysis is a two-step process. First, the samples are scanned over the range 0.5–6.0º2θ Mo (1–13º2θ Cu). This indicates which clay mineral phases are present and determines the exact diffraction angles at which textural data should be collected.

The second step of the measurement process involves the "pole-figure scan" (Ho *et al.*, 1995), in which the degree of preferred orientation of previously identified phyllosilicates was determined. The goniometer and detector were fixed at the diffraction angle corresponding to the *d* spacing of the 001 reflection of the chosen phase. Samples were then rotated around two axes, one parallel to an imaginary line connecting the goniometer and detector (designated as φ), and one normal to it (designated as ω). Diffracted X-ray intensity data were collected every 2.5º between 0 and 360º around the φ axis, and in nine steps between 0 and 40º around the ω axis. In total, 1296 intensity measurements were thus made on each sample and were corrected for grain density and specimen thickness (van der Pluijm *et al.*, 1994).

The degree of alignment was obtained from the intensity distribution of diffracted X-rays. Intensity data were displayed in pole-figure diagrams that show the distribution of crystallographic orientations in the form

https://doi.org/10.1346/CCMN.2008.0560109 Published online by Cambridge University Press

of poles to crystallographic planes. Pole-figure diagrams visualize the spatial distribution of the X-ray intensities by displaying contour lines representing the pole distribution of phyllosilicate (001) plane orientations. More aligned fabrics yield pole figures that can be contoured as concentric rings; completely random or isotropic fabrics yield figures that have no poles. The degree of particle alignment is expressed as maximum pole density in multiples of a random distribution (m.r.d.) (Wenk, 1985), where greater values reflect greater degrees of alignment. Intensity depends on the concentration of crystals aligned parallel to each other. A value for the multiples of a random distribution is produced even when the sample has not been prepared perpendicular to bedding, so a stereographic projection showing centered contour lines validates the multiples of a random distribution value.

Porosimetry

Porosities and pore-size distributions were determined on freeze-dried samples (Delage and Lefebvre, 1984) using a Micromeritics© Autopore II 9220 mercury intrusion porosimeter. The mercury-injection technique measures the bulk volume of the sample and also the pore volume into which mercury can be injected at a maximum pressure, in this case 38,000 psi (equivalent to a pore radius of ~3 nm). The measured pore volume differs from the total porosity since some pores are <3 nm radius, and some may not form part of a connected pore network. Total porosities were therefore calculated from bulk volume obtained from the mercury porosimeter, and grain-density measured using a picnometer (British Standard 733, 1987). Pore diameters were calculated from the mercury injection data assuming a mercury-air contact angle of 141º and an interfacial tension of 0.48 Nm^{-1}.

RESULTS

Porosity

Total porosities decline fairly consistently from ~10% at the top of Chochołów to 2% at the base of Bukowina Tatrzańska (Table 2, Figure 3). Mercury injection porosimetry shows that the maximum pore-throat radius in any sample is ~20 nm, consistent with the highly compacted nature of these samples (Borst, 1982; Katsube and Williamson, 1994; Schlömer and Krooss, 1997; Yang and Aplin, 1998).

Table 2. Theoretical vitrinite reflectance, porosity, and phyllosilicate fabric data.

Well and sample	Actual burial depth (m)	Estimated maximum burial depth (m)	R_c (%)	Porosity (%)	I-S maximum pole density (m.r.d.)	K+Ch maximum pole density (m.r.d.)	*d* spacing 'I-S' (Å)	*d* spacing 'K+Ch' (Å)
Chł-04	193	2393	0.57	8	3.97	3.63	10.90	7.23
Chł-06	280	2480	0.61	10	3.38	2.84	10.40	7.03
Chł-06	280	2480	0.61	10	3.80	2.98	10.15	6.97
Chł-12	514	2714	0.59	n.d.	4.61	5.43	10.87	7.22
Chł-20	821	3021	0.65	8	4.61	4.55	10.12	7.09
Chł-23	1031	3231	n.d.	5.5	4.16	4.72	11.13	7.11
Chł-28	1283	3483	0.68	4.5	5.18	5.78	10.61	7.17
Chł-38	1671	3871	0.69	n.d.	6.99	7.36	10.12	7.09
Chł-38	1671	3871	0.69	n.d.	6.87	7.44	10.22	7.01
Chł-44	2012	4212	0.70	4.5	5.67	5.68	10.24	7.26
Chł-56	2410	4610	0.75	6	5.65	6.29	10.38	7.09
Chł-60	2611	4811	0.77	4	5.00	4.96	10.38	7.09
Chł-60	2611	4811	0.77	4	5.14	5.20	10.36	7.07
Chł-66	2968	5168	n.d.	n.d.	5.78	6.23	10.46	7.11
BkT-01	102	4908	0.76	n.d.	4.92	5.27	10.56	7.18
BkT-06	294	5100	0.89	6	4.75	5.12	10.15	7.02
BkT-12	610	5416	n.d.	6	5.61	5.66	10.10	7.07
BkT-17	903	5709	1.19	3.5	5.31	5.93	10.41	7.04
BkT-23	1261	6067	1.26	n.d.	5.38	5.82	10.28	7.17
BkT-28	1595	6401	1.16	n.d.	6.13	7.00	10.15	7.04
BkT-28	1595	6401	1.16	n.d.	6.03	6.96	10.22	7.09
BkT-35	1904	6710	1.37	2	5.65	5.93	10.31	7.15
BkT-41	2201	7007	n.d.	5.5	5.94	7.18	10.36	7.15
BkT-41	2201	7007	n.d.	5.5	6.29	7.32	10.10	7.17

Porosity measured by mercury intrusion porosimetry using bulk-volume and grain-density data; R_c, the theoretical vitrinite index, calculated from the methylphenanthrene index (MPI) of Radke and Welte (1981) by Poprawa and Marynowski (2005). n.d. = not determined. The maximum pole density (in m.r.d.) as determined by HRXTG for the I-S and K+Ch peaks and their *d* spacings. Associated *d* spacings of the I-S and K+Ch peaks are given.

https://doi.org/10.1346/CCMN.2008.0560109 Published online by Cambridge University Press

Phyllosilicate fabric by XRD

Initial 2θ scans on the sample set produced well defined peaks at approximate *d* spacings of 14 Å, 10 Å, 7 Å, and 4.26 Å, corresponding to reflections for chlorite, mica, chlorite + kaolinite, and quartz, respectively. In addition, a broad peak corresponding to illite-smectite occurs between 10.12 and 11.13 Å. Pole-figure scans were obtained at two values of 2θ, one at the maximum intensity of the broad illite-smectite peak and one at a *d* spacing close to 7 Å, corresponding to the chlorite 002 + kaolinite 001 reflections. Note that no pole figure scans were made at a *d* spacing of ~10 Å, corresponding to pure mica, which is usually detrital in origin. Pole-figure scans made both at the apex of the illite-smectite peak and also on its shoulders were similar (Table 2, see data for samples Chł-06 and BkT-41), indicating that the data are not highly sensitive to the precise *d* spacing at which the pole-figure data are collected.

The maximum pole densities for both mineral peaks are recorded in Table 2. Using the presentation standard of Ho *et al.* (1999), all pole figures were processed through two smoothing cycles and rotated so that the maxima are positioned at the center of the plot, which allows all plots to refer to the same orientation.

The maximum pole densities of I-S and kaolinite+ chlorite (K+Ch) range from 2.8 to 7.4 and are very strongly correlated (Figure 4). The degree of alignment of K+Ch, which is slightly less than that of I-S at shallower burial depths, increases more rapidly than that of I-S so that they become the more aligned components at deeper burial depths (Figures 4, 5). Note that at maximum burial depths of up to ~3000 m, the 7 Å peak represents both kaolinite and detrital chlorite. Between ~3000 and 4200 m maximum burial depth, the XRD data in Table 1 suggest that kaolinite is lost and chlorite is formed. Increasingly, therefore, the 7 Å peak represents a combination of detrital and diagenetic chlorite, with a decreasing contribution from kaolinite.

The plot of maximum pole densities *vs.* depth shows two distinct trends (Figure 5). Between maximum burial depths of ~2.4 and 4 km, maximum pole densities increase from ~3 to 6, with much less change at greater depths (Figure 5). These values indicate an evolution from a modest phyllosilicate fabric to one which is very strongly aligned. One sample (Chł-38, Tables 1, 2) has a distinctly greater degree of fabric alignment than samples from similar depths. This sample has more K_2O and therefore greater clay contents than the others. This suggests that the proportion of platy clay minerals influences the extent to which phyllosilicates can be realigned with increased diagenetic grade (Curtis *et al.*, 1980), as, put simply, a larger percentage of clays relative to equidimensional grains, allows a stronger fabric to develop.

The depth range over which phyllosilicate fabrics are enhanced is also the range over which illitization occurs (Figures 2, 5, Table 1). There is thus a general correlation between the maximum pole density of I-S and the %I in I-S (Tables 1, 2), a trend which was previously noted both by Ho *et al.* (1999) for Gulf of Mexico mudstones and Worden *et al.* (2005) for North Sea mudstones. Additionally, porosity was reduced to 10% (Figure 6) before significant increases in phyllosilicate fabrics were noted.

Backscattered electron micrographs

Representative backscattered electron micrographs (Figures 7–11) illustrate the occurrence and alignment

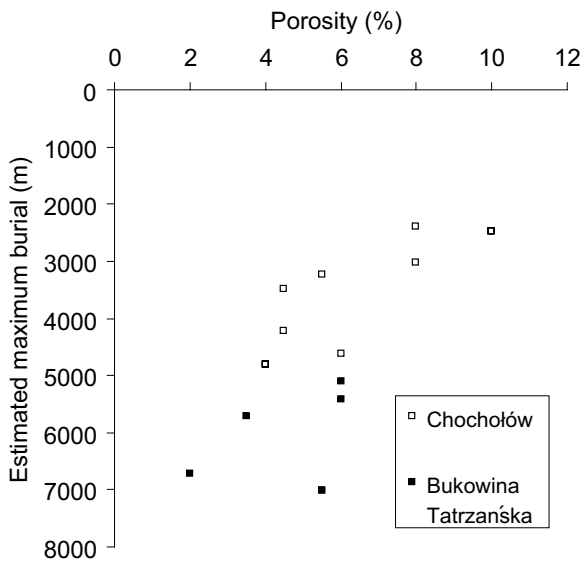

Figure 3. Porosity *vs.* estimated maximum burial depth. Open squares: Chochołów PIG-1; filled squares: Bukowina Tatrzańska PIG-1. Porosity calculated from bulk volume, mass, and grain density.

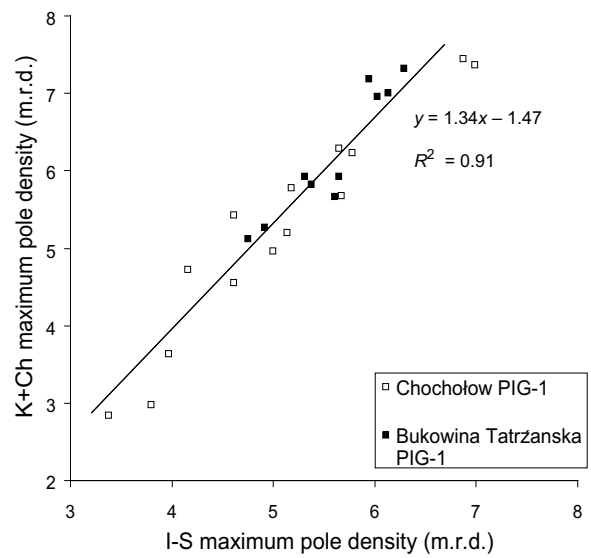

Figure 4. Maximum pole densities of I-S and K+Ch for Chochołów PIG-1 and Bukowina Tatrzańska PIG-1.

https://doi.org/10.1346/CCMN.2008.0560109 Published online by Cambridge University Press

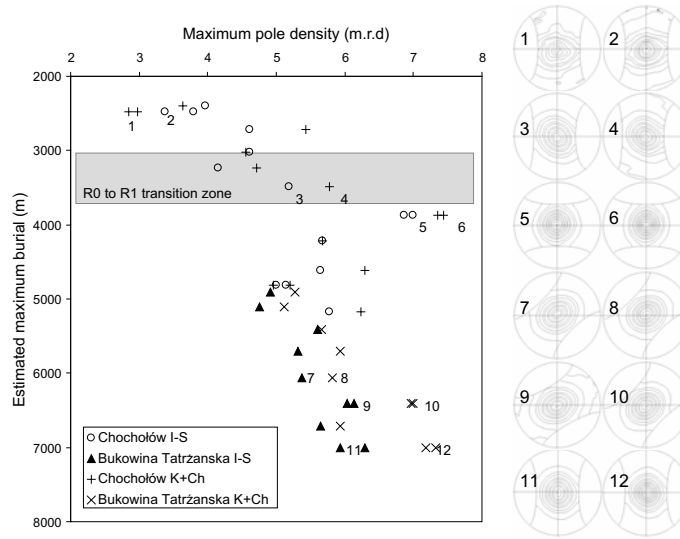

Figure 5. Maximum pole densities as a function of depth. ○: maximum pole densities of I-S in Chochołów PIG-1 samples; ▲: maximum pole densities of I-S in Bukowina Tatrzańska PIG-1 samples; +: maximum pole densities of K+Ch in Chochołów PIG-1; × : maximum pole densities of K+Ch in Bukowina Tatrzańska PIG-1. To the right, representative illite-smectite and chlorite-kaolinite pole figures are also displayed for six depth intervals. The numbers of these samples are shown on the main figure.

of detrital quartz, mica, and chlorite, the phyllosilicate groundmass and early diagenetic minerals such as framboidal and euhedral pyrite.

The back-scattered electron (BSE) images provide visual support for the fabric-alignment data, albeit on a smaller physical scale and most clearly for larger, detrital micas and chlorite. The visually weak phyllosilicate textures in the shallower samples (Figure 7) are replaced by more strongly aligned textures at greater depth (Figure 8). Similar visual observations were made by Charpentier *et al.* (2003) in deep-water Gulf of Mexico mudstones, and by Worden *et al.* (2005) in North Sea mudstones. With increasing depth and diagenetic grade, there is a sense of greater alignment of distinct minerals. The micrographs also show both the response of detrital phases to burial and the influence of detrital phases on phyllosilicate alignment. Elongated, coarse, silt-grade micas and chlorites are aligned parallel or subparallel to bedding (Figures 7, 8), while the alignment of clay-grade phyllosilicates, even in samples which have a generally well aligned fabric, is disrupted by enforced rotation around subangular quartz grains (Figure 10).

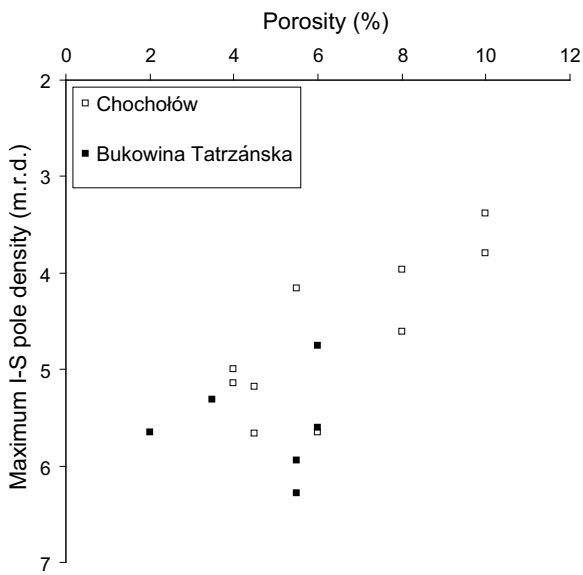

Figure 6. Porosity (%) as a function of maximum I-S pole density (m.r.d.). The porosity was calculated from the bulk volume, mass, and measured grain density.

DISCUSSION

The shallowest samples in this study have been buried to ~2.4 km and ~65ºC, have porosities of ~10%, and display modestly aligned phyllosilicate fabrics. At these temperatures, the extent of most clay-mineral diagenetic reactions will be modest. We therefore interpret our shallowest samples to be the product of mechanical compaction which reduced the porosity of the muds from a starting value of 70−80% to a value of 10% with only a partial reorientation of phyllosilicate fabric (m.r.d. of 3). The BSEM observations (Figures 7, 10) suggest that coarse-grained (>~10 μm), detrital chlorite is quite well aligned. The fabric measured at 7 Å represents the average alignment of a mixture of coarse-grained and fine-grained chlorite, plus kaolinite. Combination of the fabric and BSE data suggests that the average fabric combines a well ordered fabric for coarse-grained, detrital chlorite with a presumably less well ordered fabric for finer-grained chlorite (the kaolinite fabric is difficult to discern by BSEM). We suggest that

https://doi.org/10.1346/CCMN.2008.0560109 Published online by Cambridge University Press

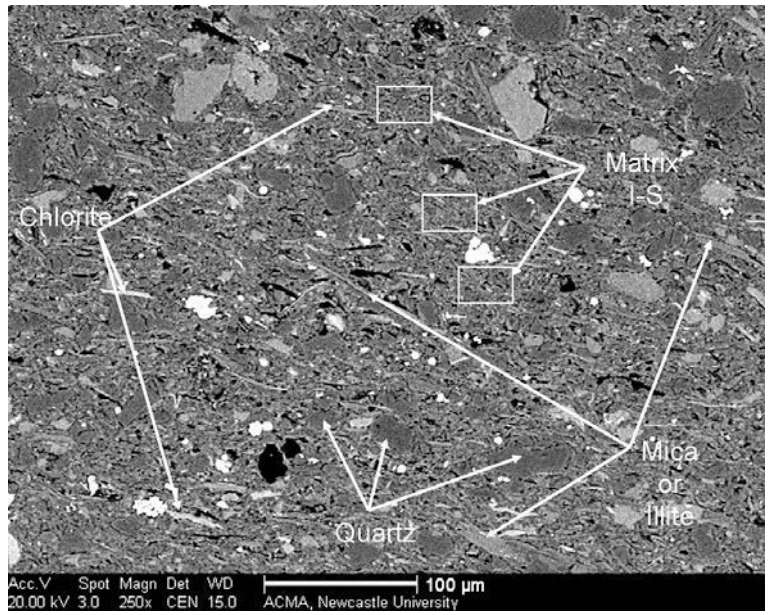

Figure 7. BSE image of Chochołów-04 (193 m, present-day burial depth). Maximum pole densities are 3.97 (m.r.d. [I-S peak]) and 3.63 (m.r.d. [K+Ch peak]).

the apparent differences in fabric alignment for coarse-grained and fine-grained chlorite reflect two depositional mechanisms, with coarser-grained particles deposited as single, aligned grains and finer-grained particles deposited as flocs or biological aggregates (Kranck and Milligan, 1985). The BSEM and fabric data suggest that similar arguments apply to coarse-grained detrital mica and finer-grained illite and illite-smectite (Figures 7, 8).

Reduction of porosity to 10% requires a considerable effective stress which can be estimated using Yang and Aplin's (2004) relationship between mudstone porosity and effective stress. Using this relationship, and assuming an average clay content of 55% (Table 1), a porosity of 10% for the shallowest Chochołów samples (Figure 3) suggests that the maximum effective stress to which these samples have been subjected is ~27 MPa (29 MPa

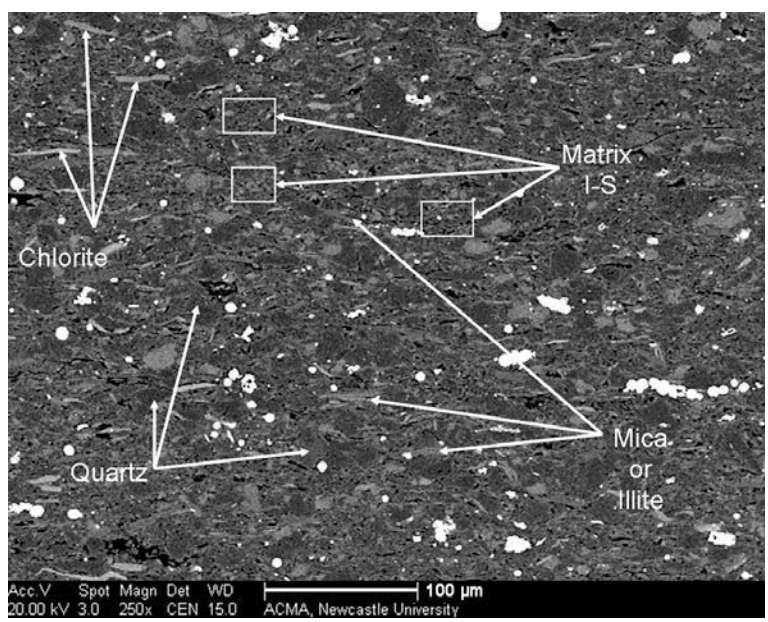

Figure 8. BSE image of Bukowina Tatrzańska-41 (2201 m, present-day burial depth). Maximum pole densities are 6.29 (m.r.d. [I-S peak]) and 7.32 (m.r.d. [K+Ch peak]).

https://doi.org/10.1346/CCMN.2008.0560109 Published online by Cambridge University Press

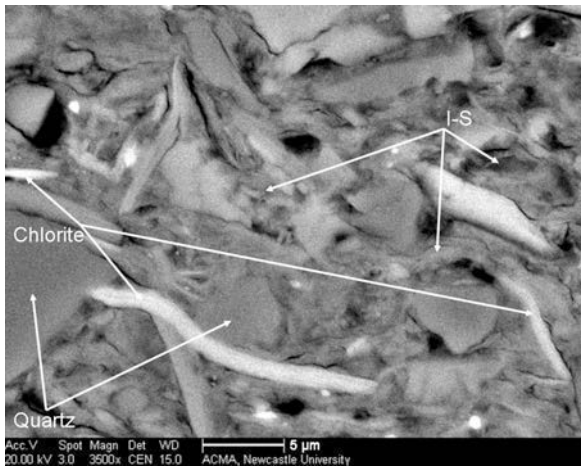

Figure 9. BSE image of Chochołów-04 (193 m, present-day burial depth). Maximum pole densities are 3.97 (m.r.d. [I-S peak]) and 3.63 (m.r.d. [K+Ch peak]). The image suggests a poorly aligned mineral matrix.

for a porosity of 8%). At a burial depth of 2.4 km (top of the Chochołów profile), the lithostatic stress is ~54 MPa and the estimated pore pressure (lithostatic stress minus effective stress) is then ~27 MPa, a little greater than the hydrostatic stress.

Although it is, in principle, possible to calculate maximum effective stresses for the lower porosity samples in Bukowina Tatrzańska, we are reluctant to do so as: (1) the relationship between porosity and effective stress is not well constrained at such low porosities; and (2) the mudstones have undergone substantial mineral diagenesis, potentially contravening the key assumption in the effective stress calculation that compaction is purely mechanical. Nevertheless, the very low porosities in the Bukowina Tatrzańska samples suggest that they have been subjected to a greater effective stress than the shallower Chochołów samples.

In our composite diagenetic profile, the trend of the alignment data is very similar to that of several mineralogical and physical parameters: rapid change is observed in the top 2000 m of the profile (2−4 km maximum burial depths), with much more gradual change in the next 3000 m (4−7 km burial). Changes in both porosity and grain density occur mainly in the upper 2 km of the profile, as do the main mineralogical changes (illitization, loss of kaolinite and K-feldspar, increase of chlorite and albite). Only quartz behaves differently, increasing from 20 to 27% at the same rate throughout the entire profile (Table 1). The mineralogical trends suggest that the overall diagenetic change may be written as:

Low-I illite-smectite + kaolinite + K-feldspar →
High-I illite-smectite + chlorite + quartz + albite

A central question in this study is the extent to which the reorientation of phyllosilicates is a purely mechanical process or whether it also reflects the chemical processes summarized above. We do not know the initial level of phyllosilicate orientation but assume, based on particle deposition models (*e.g.* Kranck and Milligan, 1985), and the visual evidence of workers such as Bennett *et al.* (1991), that the depositional fabric comprised flocs with an essentially isotropic texture, with a more aligned fabric for coarser phyllosilicates deposited as single grains. The maximum pole densities of the shallowest samples in this study are generally greater than those reported by Aplin *et al.* (2006) for Miocene-Pliocene mudstones deposited in the deep-water Gulf of Mexico and buried to similar or greater depths. The BSEM evidence suggests that, compared to the Podhale samples, the deep-water Gulf of Mexico mudstones contain less coarse-grained chlorite

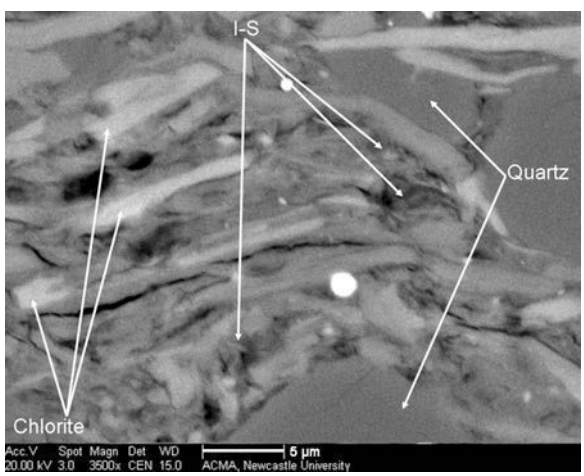

Figure 10. BSE image of Chochołów-60 (2611 m, present-day burial depth). Maximum pole densities are 5.00/5.14 (m.r.d. [I-S peak]) and 4.96/5.20 (m.r.d. [K+Ch peak]). The image suggests a moderately aligned mineral matrix.

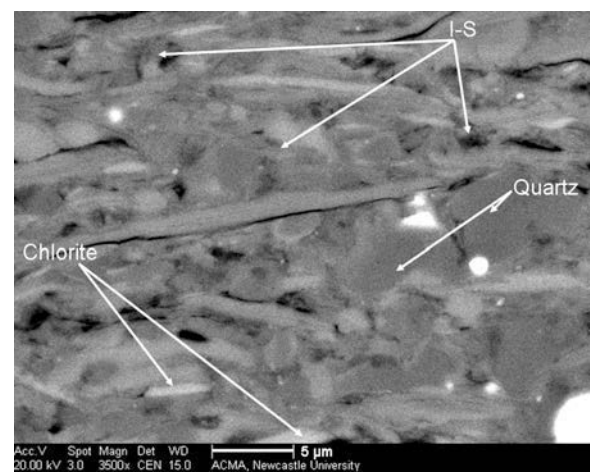

Figure 11. BSE image of Bukowina Tatrzańska-41 (2201 m, present-day burial depth). Maximum pole densities are 6.29 (m.r.d. [I-S peak]) and 7.32 (m.r.d. [K+Ch peak]). The image suggests a well aligned mineral matrix.

https://doi.org/10.1346/CCMN.2008.0560109 Published online by Cambridge University Press

and mica (compare Aplin *et al.*, 2006 with this work). We therefore interpret the somewhat stronger phyllosilicate alignment in the Podhale samples as a reflection of the grain size of the phyllosilicates, and the fact that a greater proportion of the Podhale phyllosilicates were deposited as well aligned, single grains. The Podhale data indicate that the orientation of platy minerals must have increased slowly in the (now eroded) upper 2 km of burial – from a probable initial value of ~2 m.r.d. (previously noted by Ho *et al.* 1999) – and then much more quickly between 2 and 4 km, the zone of intense illitization; similar observations were made by Ho *et al.* (1999) for some Gulf of Mexico samples. At depths below the smectite-to-illite transition, the rate of increase of preferred orientation in the Podhale samples is much reduced, again similar to Ho *et al.*'s (1999) Gulf of Mexico data. The inference is that the reorientation of both illite-smectite and kaolinite+chlorite is somehow related to the mineralogical reactions involving these minerals.

Assuming that illitization of smectite is driven by the dissolution of K-feldspar and that the mudstone system was closed to K_2O, as shown by the stable bulk-rock values (Środoń *et al.*, 2006, Table 2), we can use the I-S data to calculate what mass fraction of the whole rock has been altered by the illitization process. The dissolution of 2.2 wt.% K-feldspar (typical of the shallow Chochołów samples) provides enough K_2O to convert an amount of I-S with 40% illite layers to I-S with 80% illite layers equivalent to ~10 wt.% of the bulk rock. Since 2:1 clays comprise ~50% of the bulk rock, the calculation shows that only ~20% of the 2:1 clays are altered by the illitization process; most of the clays are apparently unreactive. Despite this, we observe a major enhancement in the I-S phyllosilicate fabric over the depth range at which illitization occurs, implying that unreactive illitic material is reoriented along with the reactive I-S. This conclusion is supported by a detailed examination of the orientation data presented in Table 2. At a given depth, the m.r.d. value of the I-S is independent of the peak *d* spacing (*e.g.* compare closely located samples Chł-04 and -06, -20, and -23 or BkT-01 and -06). In terms of the overall diffraction effect, peaks closer to 10 Å indicate an increasingly dominant influence of discrete illite over I-S. The lack of a correlation between alignment and *d* spacing for samples at similar depths suggests that both reactive I-S and unreactive illite are oriented to similar degrees, both in shallow and deeper samples (illite slightly more, as indicated by double measurements on samples Chł-06 and BkT-41). We conclude that both reactive illite-smectite and inert illite were reoriented to a similar degree over the depth range of illitization.

Between 4.5 and 7 km, where illitization has ceased due to the exhaustion of K-feldspar (Table 1, compare also the plots of Środoń *et al.*, 2006), the orientation of both I-S and chlorite continues to increase, but at a much slower rate than within the illitization window (Table 1, Figure 5). A satisfactory model of the reorientation process must explain all the observations outlined above, as well as the striking similarity of the orientation indices measured from the illite-smectite and kaolinite-chlorite reflections (Figure 4).

We suggest that the reorientation of platy particles under stress in a rock of a given mineralogical and granulometric composition results from the interplay of several factors including: (1) the magnitude and direction of the principal effective stress; (2) mineralogical transformations; (3) the porosity required for particle realignment and growth; and (4) the presence of lubricating water. In the absence of reactive illite-smectite, the rate of mechanical reorientation would gradually decrease as porosity and water was lost. However, the illitization of smectite is a water-producing mineral reaction (Hower *et al.* 1976; Boles and Franks, 1979). At the temperature-pressure-salinity range of smectite illitization, Na-smectite exists as a 2-water-layer complex (1.5 nm) (Colten, 1985) and Ca-smectite probably as a 3-layer (1.75 nm) complex. A volume V of smectite converted to illite thus generates $0.5-0.75\ V$ of water. We suggest that the generation of water-filled nanoporosity under conditions of elevated stress facilitates the mechanical reorientation of both reactive and non-reactive platy particles in the zone of illitization. Simultaneously, more randomly oriented, curved smectitic particles are replaced by more rigid illite particles growing normal to the maximum effective stress. Both processes will result in the enhanced orientation of illitic particles, and the relative role of the two processes will depend on the relative volumes of the reactive and non-reactive platy particles. However, we have insufficient data to speculate about the precise growth mechanisms of the neoformed illite, *e.g.* for differentiating between the formation of new crystals or, as suggested by Pevear (1999), as epitaxial overgrowths on pre-existing detrital illite grains.

The potential reorientation mechanisms outlined above also explain the strong correlation between the fabric alignment of the 7 Å K+Ch phases and the I-S phase (Figure 4), and the major enhancement of the K+Ch fabric within the illitization zone between 2.4 and 4.6 km (Figure 5). The initial, poorly aligned fabric of the K+Ch reflects the mode of deposition of the minerals, as for the I and I-S phases. We interpret the strong enhancement of fabric in the illitization window, which is even more marked than that of the I and I-S phases, as a result of (1) the loss of poorly aligned kaolinite and (2) the growth of neoformed chlorite crystals, oriented normal to the maximum effective stress. Petrography shows that kaolinite in shallower samples occurs mainly in the fine-grained 'matrix', assumed to be deposited with an isotropic fabric. The loss of kaolinite will in itself enhance the average alignment of the K+Ch phases since coarse-grained detrital chlorite is well aligned as a result of its

https://doi.org/10.1346/CCMN.2008.0560109 Published online by Cambridge University Press

depositional habit (Figures 7, 8). The neoformation of chlorite with the crystal orientation normal to the maximum stress further enhances the fabric.

Below the illitization window, despite an additional 3 km burial and a possible increase in effective stress of ~30 MPa, the rate of reorientation of phyllosilicates slows markedly and perhaps halts (Figure 5). Taking the data as a whole and extrapolating back to the most likely depositional m.r.d. values of ~2, the main zone of phyllosilicate fabric alignment clearly occurs over the main I-S transition zone (Figure 5). These results are very similar to those reported by Ho *et al.* (1999) in a series of shallow-water Gulf of Mexico mudstones but differ from those presented by Aplin *et al.* (2006) from a series of deep-water Gulf of Mexico mudstones where much less fabric realignment was observed over the depth and temperature range at which illitization occurs. These different observations are not easily reconciled, although noteworthy is that both the diagenetic trends in the deep-water Gulf of Mexico samples and the pore-pressure regime of the area are rather different from those in the Podhale Basin. In the deep-water Gulf of Mexico samples, smectite persists in the <0.2 μm fractions to temperatures of 127ºC and R1 I-S with 30–40% smectite layers occurs at all depths between 3 and 5.5 km. Generally, therefore, there is less evidence for illitization in the Gulf of Mexico sample set, despite their deep burial and relatively high temperature. Furthermore, despite their deeper burial, high over-pressures in the Gulf of Mexico have restricted compaction such that the porosities of those mudstones are between 15 and 20%. The greater porosities of the Gulf of Mexico samples indicate that, despite their current burial depth of 4–5.5 km, the smectite-to-illite transition is occurring in a smaller effective stress (and greater pore pressure) regime than the Podhale samples. One possibility is, therefore, that the extent to which neoformed clay minerals are realigned perpendicular to the maximum effective stress is a function of the differential effective stress. In a highly overpressured slope setting, such as the deep-water Gulf of Mexico, a more isotropic stress regime may have resulted in a more isotropic clay mineral fabric.

CONCLUSIONS

In this work we have attempted to unravel the relative importance of (1) sedimentation, (2) mechanical compaction, and (3) clay mineral diagenesis in the phyllosilicate fabric of a suite of rapidly deposited, relatively homogeneous, fine-grained mudstones from the Podhale Basin. At a depth of ~2.4 km, and an effective stress of ~27 MPa, mechanical compaction has reduced porosity from an initial value of ~75% to 10%. High-resolution X-ray texture goniometry shows that this major loss of porosity has resulted in only a relatively modest alignment of the bulk phyllosilicate mineral assemblage. However, BSE images suggest that relatively coarse-grained chlorite and mica (>~10 μm) are quite strongly aligned, which we interpret as the result of their sedimentation as single grains. In contrast, finer-grained phyllosilicates are deposited as isotropic flocs or aggregates, and are not substantially realigned by mechanical compaction. Between ~2.4 and 4 km, a major realignment of both I-S and chlorite occurs perpendicular to the principal (vertical) effective stress, concomitant with the illitization of smectite and the related loss of kaolinite, and the formation of diagenetic chlorite. These data support the idea that illitization is a nanoscale dissolution-reprecipitation process, and that neoformed clay mineral phases grow predominantly normal to the maximum stress. We propose that in the zone of illitization, the generation of water and nanoporosity under conditions of elevated stress facilitates the mechanical reorientation of both reactive and non-reactive platy particles. The degree of phyllosicilate alignment is further influenced by the clay-quartz ratio of the sample and perhaps by the anisotropy of the stress field. In these samples, the exhaustion of reactive K-bearing phases at ~5 km burial depth halted the illitization process at 80% illite layers. Despite a further 2.5 km of burial and temperatures up to 160ºC, little or no further enhancement of phyllosilicate fabric occurs, reinforcing the notion that at low porosities realignment of phyllosilicates requires mineralogical change in an anisotropic stress field.

ACKNOWLEDGMENTS

We thank the UK Natural Environment Research Council and BP for supporting RJD-S's PhD studies; reviewers David Pevear and Richard Worden, plus Associate Editor Doug McCarty, provided helpful and insightful comments.

REFERENCES

Anczkiewicz, A. (2006) Verification by AFT technique of the maximum paleotemperatures evaluated from illite-smectite for the Tatra Mts., the Podhale Basin, and the neighboring area of the Outer Carpathians. PhD thesis, Institute of Geological Sciences PAN, Krakow (in Polish).

Aplin, A.C., Matenaar, I.F., McCarty, D., and van der Pluijm, B.A. (2006) Influence of mechanical compaction and clay mineral diagenesis on the microfabric and pore-scale properties of deep water Gulf of Mexico mudstones. *Clays and Clay Minerals*, **54**, 501–515.

Bennett, R.H., O'Brien, N.R., and Hulbert, H. (1991) Determinants of clay and shale microfabric signatures: Processes and mechanisms. Pp. 5–33 in: *Microstructure of Fine-Grained Sediments* (R.H. Bennett, W.R. Bryant, and M.H. Hulbert, editors), Springer Verlag, Berlin.

Boles, J.R. and Franks, S.G. (1979) Clay diagenesis in Wilcox Sandstones of southwest Texas. *Journal of Sedimentary Petrology*, **49**, 55–70.

Borst, R.L. (1982) Some effects of compaction and geological time on the pore parameters of argillaceous rocks. *Sedimentology*, **29**, 291–298.

Bowles, F.A., Bryant, W.R., and Wallin, C. (1969)

Microstructure of unconsolidated and consolidated marine sediments. *Journal of Sedimentary Petrology*, **39**, 1546–1551.

British Standards 733, part 2 (1987) *Pyknometers. Part 2. Methods for calibration and use of pyknometers*. British Standard Institution, London.

Charpentier, D., Worden, R.H., Dillon, C.G., and Aplin, A.C. (2003) Fabric development and the smectite to illite transition in Gulf of Mexico mudstones: an image analysis approach. *Journal of Geochemical Exploration*, **78–79**, 459–463.

Colten, V.A. (1985) Experimental determination of smectite hydration states under simulated diagenetic conditions. PhD thesis, University of Illinois, Urbana, Illinois, USA, 144 pp.

Curtis, C.D., Lipshie, S.R., Oertel, G., and Pearson, M.J. (1980) Clay orientation in some Upper Carboniferous mudrocks, its relationship to quartz content and some inferences about fissility, porosity and compactional history. *Sedimentology*, **27**, 333–339.

Delage, P. and Lefebvre, G. (1984) Study of a sensitive Champlain Clay and its evolution during consolidation. *Canadian Geotechnical Journal*, **21**, 21–35.

Hedberg, H.D. (1936) Gravitational compaction of clays and shales. *American Journal of Sciences*, **31**, 241–287.

Ho, N.C., Peacor, D.R., and van der Pluijm, B.A. (1995) Reorientation of phyllosilicates in the mudstone-to-slate transition at Lehigh Gap, Pennsylvania. *Journal of Structural Geology*, **17**, 345–356.

Ho, N.C., Peacor, D.R., and van der Pluijm, B.A. (1999) Preferred orientation of phyllosilicates in Gulf Coast mudstones and relation to the smectite-illite transition. *Clays and Clay Minerals*, **47**, 495–504.

Ho, N.C., van der Pluijm, B.A., and Peacor, D.R. (2001) Static recrystallization and preferred orientation of phyllosilicates: Michigamme Formation, northern Michigan, USA. *Journal of Structural Geology*, **23**, 887–893.

Hower, J., Eslinger, E.V., Hower, M.E., and Perry, E.A. (1976) Mechanism of burial metamorphism of argillaceous sediment.1. Mineralogical and chemical evidence. *Geological Society of America Bulletin*, **87**, 725–737.

Jacob, G., Kisch, H.J., and van der Pluijm, B.A. (2000) The relationship of phyllosilicate orientation, X-ray diffraction intensity ratios, and c/b fissility ratios in metasedimentary rocks of the Helvetic zone of the Swiss Alps and the Caledonides of Jamtland, central western Sweden. *Journal of Structural Geology*, **22**, 245–258.

Katsube, T.J. and Williamson, M.A. (1994) Effects of diagenesis on shale nano-pore structure and implications for sealing capacity. *Clay Minerals*, **29**, 451–461.

Kotarba, M. (2003) Diagenetic history of illite/smectite in clay rocks of Western Carpathians (Krakow-Zakopane transect). PhD thesis, Institute of Geological Sciences PAN, Krakow, (in Polish) 198 pp.

Kranck, K. and Milligan, T.G. (1985) Origin of grain-size spectra of suspension deposited sediment. *Geo-Marine Letters*, **5**, 61–66.

Kranck, K., Smith, P.C., and Milligan, T.G. (1996) Grain-size characteristics of fine-grained unflocculated sediments. 1. 'One-round' distributions. *Sedimentology*, **43**, 589–596.

O'Brien, N.R. and Slatt, R.M. (1990) *Argillaceous Rock Atlas.* Springer-Verlag, New York.

Oertel, G. and Curtis, C.D. (1972) Clay-ironstone concretion preserving fabrics due to progressive compaction. *Geological Society of America Bulletin*, **83**, 2597–2606.

Olszewska, B.W. and Wieczorek, J. (1998) The Paleogene of the Podhale Basin (Polish Inner Carpathians) – micropaleontological perspective. *Przegląd Geologiczny*, **46**, 721–728 (in Polish).

Poprawa, P. and Marynowski, L. (2005) Thermal history of the Podhale Trough (northern part of the Central Carpathian Paleogene Basin) – preliminary results from 1-D maturity modeling. *Mineralogical Society of Poland – Special Papers*, **25**, 352–355.

Radke, M. and Welte, D.H. (1981) The Methylphenanthrene Index (MPI): A maturity parameter based on aromatic hydrocarbons. Pp. 504–512 in: *Advances in Organic Geochemistry 1981* (M. Bjøroy, editor). J. Wiley, New York.

Schlömer, S. and Krooss, B.M. (1997) Experimental characterisation of the hydrocarbon sealing efficiency of cap rocks. *Marine and Petroleum Geology*, **14**, 565–580.

Środoń, J., Morgan, D.J., Eslinger, E.V., Eberl, D.D., and Karlinger, M.R. (1986) Chemistry of illite/smectite and end-member illite. *Clays and Clay Minerals*, **34**, 368–378.

Środoń, J., Drits, V.A., McCarty, D.K., Hsieh, J.C.C., and Eberl, D.D. (2001) Quantitative X-ray diffraction analysis of clay-bearing rocks from random preparations. *Clays and Clay Minerals*, **49**, 514–528.

Środoń, J., Kotarba, M., Biroň, A., Such, P., Clauer, N., and Wójtowicz, A. (2006) Diagenetic history of the Podhale-Orava Basin and the underlying Tatra sedimentary structural units (Western Carpathians): evidence from XRD and K-Ar of illite-smectite. *Clay Minerals*, **41**, 751–774.

Tari, G., Báldi, T. and Báldi-Beke, M. (1993) Paleogene retroarc flexural basin beneath the Neogene Pannonian Basin: a geodynamic model. *Tectonophysics*, **226**, 433–455.

van der Pluijm, B.A., Ho, N.-C., and Peacor, D.R. (1994) High-resolution X-ray texture goniometry. *Journal of Structural Geology*, **16**, 1029–1032.

Vasseur, G., Djeran-Maigre, I., Grunberger, D., Rousset, G., Tessier, D. and Velde, B. (1995) Evolution of structural and physical parameters of clays during experimental compaction. *Marine and Petroleum Geology*, **12**, 941–954.

Wenk, H.-R., (1985) Measurement of pole figures. Pp. 11–48 in: *Preferred orientation in deformed metals and rocks: An introduction to modern texture analysis* (H.-R. Wenk, editor). Academic Press, London.

Wieczorek, J. (1989) Model Hecho dla fliszu podhalańskiego? *Przeglad Geologiczny*, **37**, 419–423.

Worden, R.H., Charpentier, D., Fisher, Q.J., and Aplin, A.C. (2005) Fabric development and the smectite to illite transition in Upper Cretaceous mudstones from the North Sea: an image analysis approach. Pp. 103–114 in: *Understanding the Micro to Macro Behaviour of Rock-Fluid Systems* (R.P. Shaw, editor). Special Publication, **249**, Geological Society, London.

Yang, Y.L. and Aplin, A.C. (1998) Influence of lithology and compaction on the pore size distribution and modelled permeability of some mudstones from the Norwegian Margin. *Marine and Petroleum Geology*, **15**, 163–175.

Yang, Y.L. and Aplin, A.C. (2004) Definition and practical application of mudstone porosity-effective stress relationships. *Petroleum Geoscience*, **12**, 153–162.

(*Received 27 February 2007; revised 26 September 2007; Ms. 1225; A.E. Douglas K. McCarty*)